

Ra's Abdah of the north Eastern Desert of Egypt: the role of granitic dykes in the formation of radioactive mineralization, evidenced by zircon morphology and chemistry

Ali A. Omran¹ · Osama K. Dessouky¹

Received: 29 September 2015 / Revised: 29 February 2016 / Accepted: 15 March 2016 / Published online: 23 March 2016
© Science Press, Institute of Geochemistry, CAS and Springer-Verlag Berlin Heidelberg 2016

Abstract Syenogranitic dykes in the north of Egypt's Eastern Desert are of geological and economic interest because of the presence of magmatic and supergene enrichment of radioactive mineralization. Zircon crystal morphology within the syenogranitic dykes allows precise definition of sub-alkaline series granites and crystallized at mean temperature of about 637 °C. The growth pattern of the zircons suggest magmatic and hydrothermal origins of radioactive mineralization. Hydrothermal processes are responsible for the formation of significant zircon overgrowth; high U-zircon margins might have occurred contemporaneously with the emplacement of syenogranitic dykes which show anomalous uranium (eU) and thorium (eTh) contents of up to 1386 and 7330 ppm, respectively. Zircon chemistry revealed a relative increase of Hf consistent with decreasing Zr content, suggesting the replacement of Zr by Hf during hydrothermal activity. Visible uranium mineralization is present and recognized by the presence of uranophane and autunite.

Keywords Syenogranitic dykes · Zircon · Morphology · Typology · Uranium · Egypt

1 Introduction

The role of felsic intrusions in the formation of post magmatic (hydrothermal) mineral deposit types is unquestionable, and mineralization associated with the

systems are frequently localized and proximal to granitic cupolas and (or) zones with a high density of dykes (Moore 1975; Derre et al. 1986; Breiter 2002; Vallance et al. 2003; Lentz 2005; Štemprok et al. 2008; Bineli Betsi and Lentz 2010).

Zircon, being highly resistant to chemical and physical influences, is a particularly useful mineral for petrological investigations. It is one of the most widely used minerals for understanding the petrogenesis of magmatic, metamorphic, and sedimentary rocks (Corfu et al. 2003). Moreover, links between zircon growth and granitoid petrology have been argued in various studies.

Ra's Abdah is an example of the important relationship between magmatic intrusions and the localization of radioactive mineralization. The area under investigation was first reported to be radioactive by Omran (2005). Omran (2015) argued the high radioactivity measurements to poly-mineralized microgranite dykes invaded the older granitoid rocks. Here we present new data on the radioactive mineralization restricted to the syenogranitic dykes using zircon morphology, typology, and chemistry studies.

2 Geologic background and petrographic inferences

Generally, basement rocks of Egypt underlie the north-western part of the Arabian-Nubian shield: the eastern limb of the U-shaped Pan-African fold belt that girdles the continent of Africa. The Egyptian sector of the Nubian-Arabian Shield (Eastern Desert of Egypt and Sinai) is essentially formed by metamorphosed oceanic-type basalts and island-arc to calc-alkaline igneous suites intruded by granitic batholiths (Kroner et al. 1990; Stein and Goldstein

✉ Osama K. Dessouky
Osamakhairy25@gmail.com

¹ Nuclear Materials Authority, P.O. Box 530, El Maadi, Cairo, Egypt

1996). These granites are intruded by basic-acidic dyke swarms, which are related to an extensional tectonic regime developed during the late stages of the Pan-African cycle (Stern et al. 1984; Stern and Hedge 1985).

The studied area is located approximately 20 km southwest of Safaga City on the Red Sea between $26^{\circ}42'50''$ and $26^{\circ}44'28''$ N and $33^{\circ}44'51''$ and $33^{\circ}47'59''$ E (Fig. 1). It consists of Precambrian basement rocks including older granitoids, younger gabbro, younger granites, and mafic and felsic dykes (the subject of the present work). Older granitoids are considered the oldest rock in the area of study, and range in composition from granodiorite to quartz diorite. Younger gabbros crop out at the northwestern part of the study area surrounding Wadi Abu Hadidah. These rocks form moderate-to-low relief hills. Younger gabbro intrudes the older granitoids and is intruded by felsic dykes. Younger granites are mainly represented by small elliptical masses in the western part of the mapped area.

2.1 Dyke phases

The basement rocks of the study area are traversed by dykes which are emplaced along regional fractures varying in composition from felsic to mafic. These dykes show pronounced variation in direction. Based on field observations and cross-cutting relationships between the different dyke varieties, the studied dykes can be classified into two phases: early phase and late-stage phase. The early

phase includes a series of mafic dykes, which are the oldest and most prevalent. These are unmetamorphosed and occur in closely parallel sets forming swarms. They are mainly basaltic in composition and trend WNW, NW, and NE in decreasing order of abundance.

In the studied area, only basaltic dykes invade the Precambrian basement, never felsic ones (Fig. 2). They have a distinct thickness from centimeters to five meters, extend for several kilometers beyond the limit of the study area, and generally show sharp contacts with the older granitoid rocks. Generally, these dykes are massive and range from black to greyish-green in color.

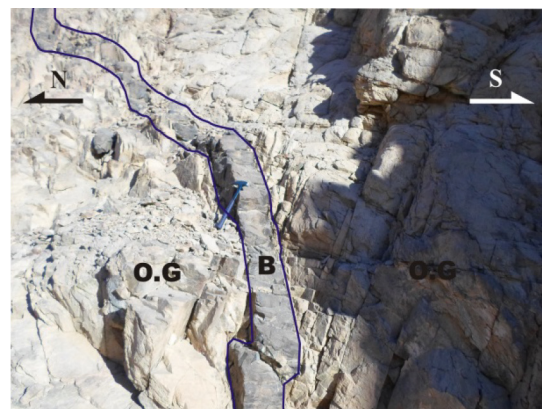


Fig. 2 General view showing basaltic dyke *B* extruding older granitoids (O.G.)

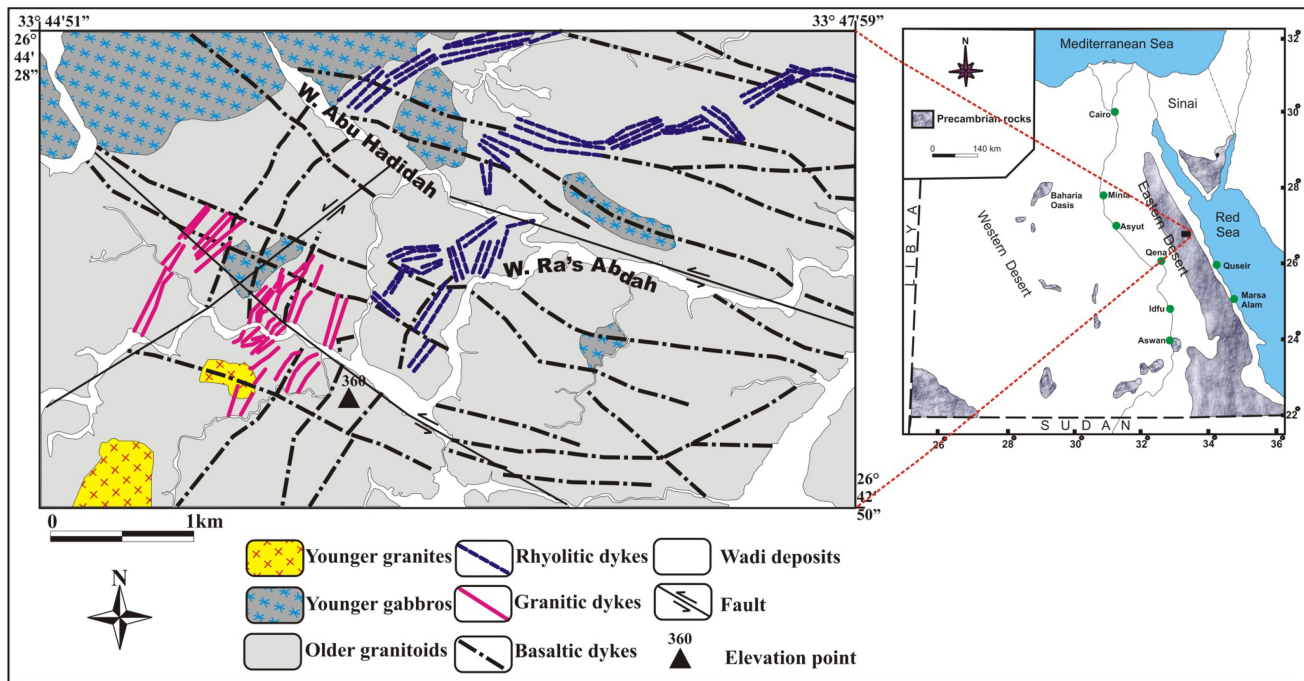


Fig. 1 Geologic map of the studied area, north Eastern Desert of Egypt



Fig. 3 General view showing syenogranitic dyke (G) as well as basaltic dyke invading older granitoids (O.G)



Fig. 4 General view showing syenogranite dykes G intersect older granoitoids (O.G)



Fig. 5 Close up view showing manganese dendrites associated with syenogranite dykes

The late-stage phase (felsic) dykes are represented by rhyolitic and granitic dykes. The rhyolitic dykes often occupy the middle part of the investigated area. They are highly weathered and form huge separated blocks in some parts. The rhyolitic dykes are fine-grained with massive appearance and are red to pink in color.

The granitic dykes are less abundant than the rhyolite. They are restricted only to a highly deformed, faulted, and sheared narrow zone, 100 to 300 m in width and extending for more than 1.5 km in a NE to NNE direction. The zone has been split and dislocated into two parts under the action of a NW–SE left lateral strike-slip fault. The predominant host rocks of these dykes are the older granitoids and, to a lesser extent, younger gabbros. Generally, the granitic dykes show an extrusive relationship with the older granitoids (Figs. 3 and 4), and were emplaced along pre-existing structures during their ascent. No xenoliths from the country rock are clearly observed within these dykes. The dykes vary from sub-vertical to vertical and are inclined with elliptical shaped bodies. Their outcrop dimensions range from a few meters to 100 m in length and from less than a meter up to tens of meters in width. These dykes have been affected by local strike-slip and normal faults leading to margin alteration in some parts. In other parts, these dykes show ample evidence of later hydrothermal activity through which several generations of fracture-filling veins consisting of quartz, chlorite, and epidote have developed in association with alteration of the wallrock including ferrugination, silicification, episyenitization, koalinization, and the formation of manganese dendrites (Fig. 5). Individual granite dykes generally strike NE-SW, which is approximately compatible with the trend of predominating structure.

Microscopically, this rock is mainly of syenogranitic composition and sometimes shows alkali feldspar granite varieties, with diagnostic aluminous minerals, equigranular texture, and fine-to medium grain size. The rock is essentially composed of alkali feldspars (about 52.7 %), quartz (about 32.5 %), and plagioclase (less than 10.1 %), with subordinate amounts of biotite (about 1.8 %) and muscovite (about 1.2 %). On the other hand, the rock is highly charged with zircon (Fig. 6), and Iron oxy-hydroxides in addition to radioactive minerals which represent the main accessories.

3 Zircon morphology

Zircon represents the main accessory mineral in the studied rock and ranges in concentration from 1646 ppm to more than 10,000 ppm (Omran 2015). Nine samples were collected from syenogranitic dykes for zircon studies. After separation, they were studied under the binocular microscope in order to exclude the damaged crystals, and to define morphological types and sub-types, color, and internal structures. Based on Pupin's (1980) deductions, for accurate conclusions, the examined zircon crystals should exceed one hundred unbroken crystals for each sample. Only in four samples were we able to achieve this

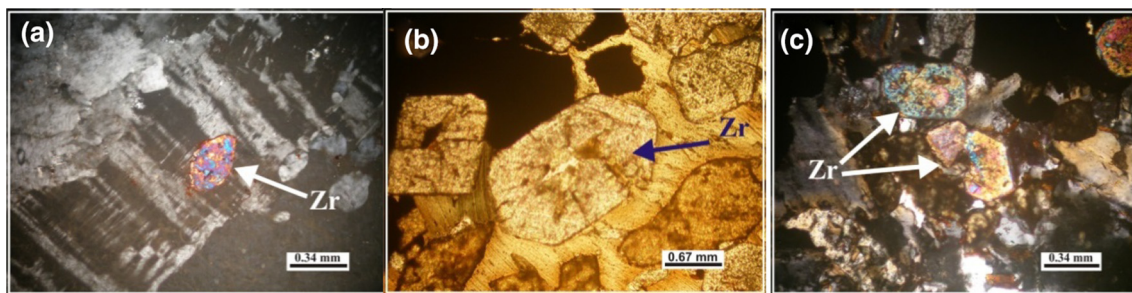
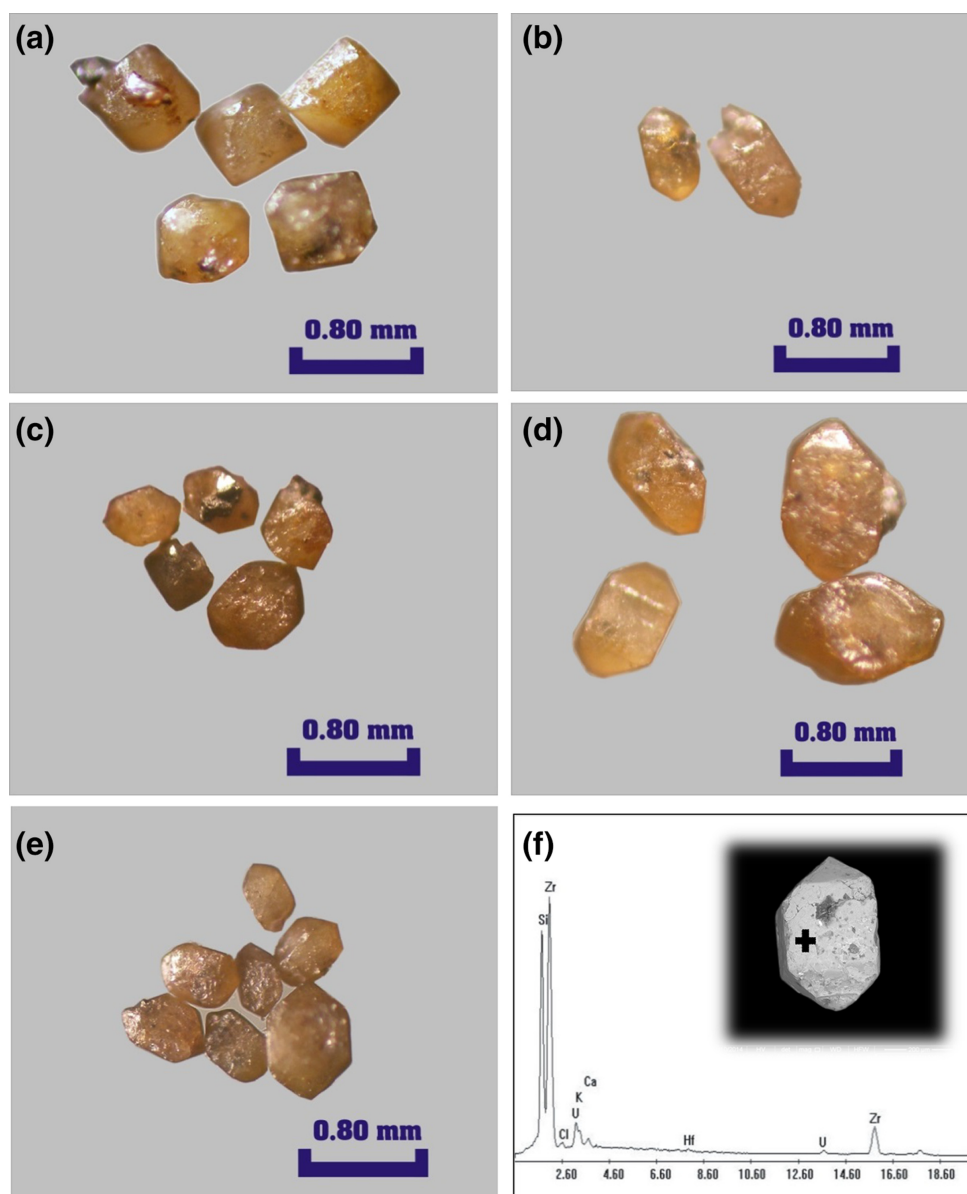


Fig. 6 Photomicrographs showing euhedral zircon crystals (Zr) in syenogranite dykes. **a** Plagioclase enclosing minute crystal of zircon, C.N. **b** Euhedral crystal of zircon in syenogranite dykes, P.L. **c** Cracked zircon crystals enclosing inclusions, C.N

Fig. 7 Photomicrograph of different types of separated euhedral zircon grains from different samples of syenogranite dykes. **a, c and d** are showing slightly overgrowth of zircon grains, **f** is SEM analyses of the studied zircon



requirement. The present morphological studies including zircon typology were carried out over more than 538 grains of zircon, separated from four chosen samples of

syenogranite dykes. The samples were photographed by SEM in order to observe the details of the crystalline forms and the external structures (overgrowth, corrosion

Fig. 8 Crystal morphology characteristics of zircon (SEM) from different samples of the studied syenogranitic dykes. Category **a** zircon crystals showing the development of pyramid {101} \gg {211} and prism {100} $>$ {110}, which are belong to S20. **b** zircon crystals showing the development of pyramid {101} \gg {211} and prism {100} \gg {110} which are belong to S25. **c** zircon crystals showing the development of pyramid {101} \gg {211} and prism {100} \gg {110} which are belong to subtype S24. **d** zircon crystals showing the development of pyramid {101} \gg {211} and prism {100} = {110} which are belong to S15. **e** few samples of zircon crystals belonging to P5, S14 and S19 respectively

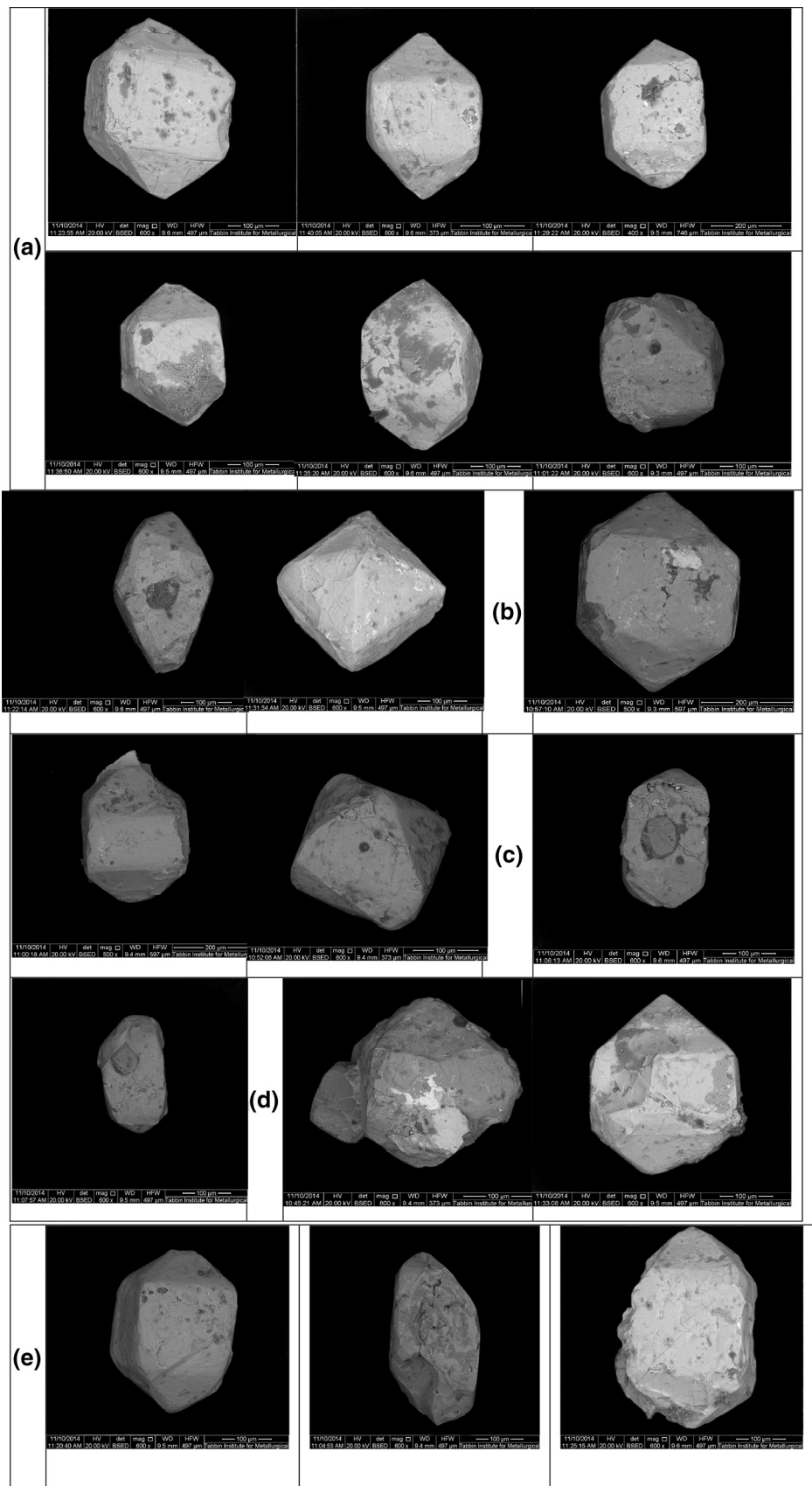


Fig. 9 **a** photomicrograph shows embayment into low-U regions in the zircon crystals (SEM), the white arrow pointed to uranophane as inclusions. **b** EDX for the detected uranophane inclusion in zircon

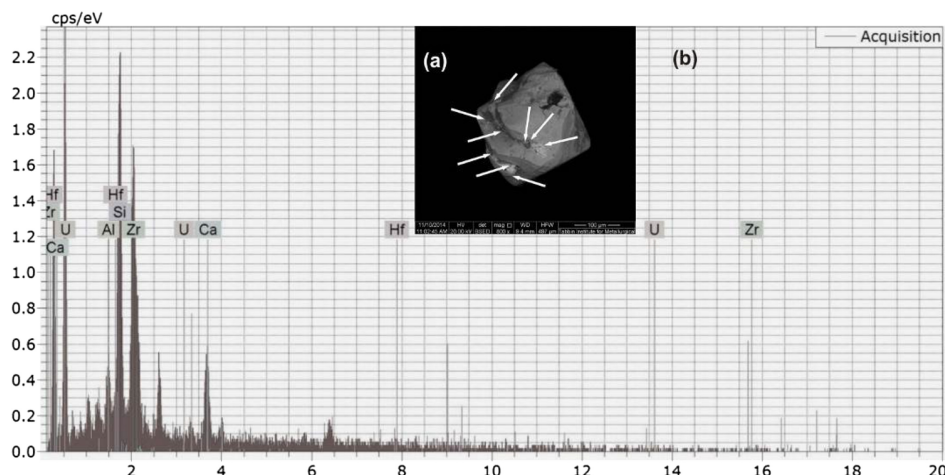
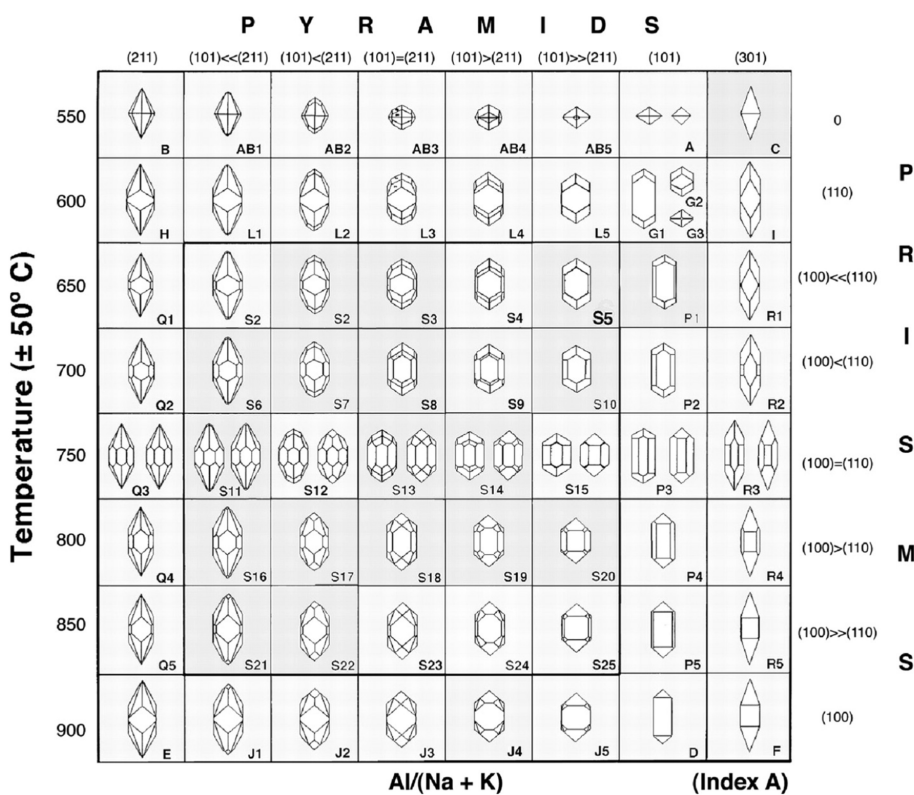


Fig. 10 Zircon typological classification and corresponding geothermometric scale proposed by Pupin (1980). Index A reflects the Al/alkali ratio, controlling the development of zircon pyramids, whereas temperature affects the development of different zircon prisms



features). The studied zircon grains range in color from pale yellow to bright yellow, honey, and brown (Fig. 7). Some zircon crystals show significant overgrowth features (Figs. 7, 8 category c, d).

However, most zircons fall into general color series of increasing radiation damage, pale yellow, straw, honey, brown, and black (Gastil et al. 1967). In addition to radiation damage, the color may also be affected by trace element inclusion content.

Zircon is tetragonal and most commonly grows as doubly-terminated prismatic crystals with elongation

(length-to-width) ratios ranging from 1 to 5. This ratio is commonly believed to reflect crystallization velocity. Indeed, needle-shaped acicular zircon crystals are common in rapidly crystallized, porphyritic, sub-volcanic intrusions; high-level granites; and gabbros, whereas stubby and equant forms are more common in deep-seated, slowly cooled intrusions (Fig. 8b, d). Some of the studied zircon grains show elongation (Fig. 8c), suggesting a high fluid content of the magma and confirming the magmatic origin (Pupin et al. 1978; Dardier 1999; El-Mansi et al. 2004).

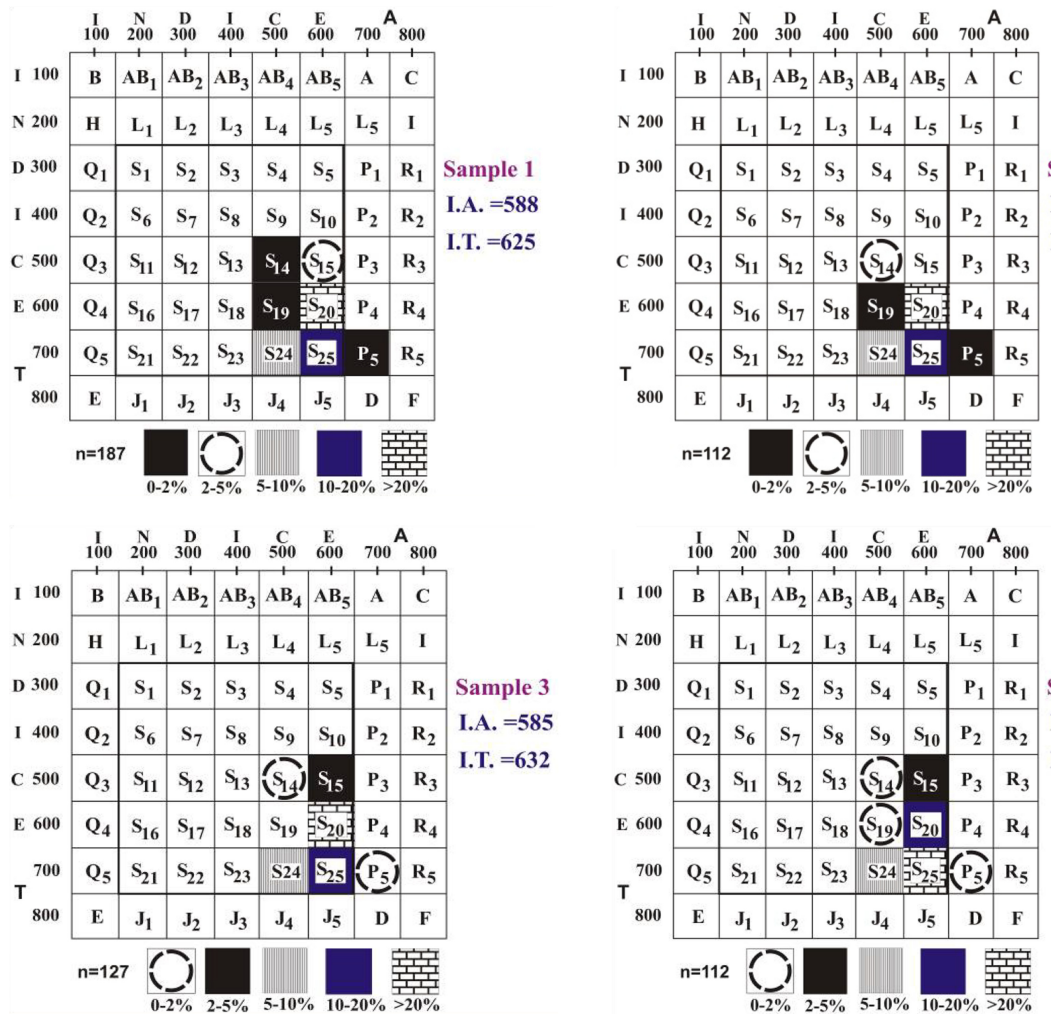


Fig. 11 Typologic frequency distribution of syenogranite zircons in the study area, n = the number of investigated zircon crystals

Hydrothermal zircon growth has been described during late-stage magmatic or post-magmatism crystallization (Rubin et al. 1989). The main characterization is the formation of high-U zircon margins, which in some cases form simple overgrowths, but more commonly are embayed into low-U regions in the zircon crystals (Fig. 9). These high-U regions may have formed by recrystallization, or dissolution and re-precipitation during an event, which probably was accompanied by regional hydrothermal activity.

A zircon xenocrystic core occurs simply when a previously crystallized zircon is surrounded by later crystallized one, possibly generated during late-stage crystallization; the older zircon becomes a xenocrystic core in the newly formed zircon (Fig. 8c). The presence of zircon cores is associated sometimes with iron oxy-hydroxides as well as allanite and could be attributed to the change of physico-chemical parameters of magma conditions during formation. Köksal et al. (2008), mentioned that, zircon typology

method proposed by Pupin (1980) arranges morphological types of zircon on the zircon typologic diagram based on the relative development of {100} and {110} prisms and {101} and {211} pyramids (Fig. 10). Chemical composition of the melt affects the relative growth of zircon pyramids according to Pupin (1980). For example, the {211} pyramid dominates in zircon originating in a hyperaluminous or hypoalkaline medium, while the {101} pyramid is characteristic of a hyperalkaline or hypoaluminous medium. The {301} pyramid is interpreted to be characteristic of zircon crystals formed in a potassium-rich alkaline medium (Pupin 1980). Thus, Pupin (1980) suggested that the alkaline ratio (Al) controls the A-index (A.I.) of a zircon population. Pupin (1980) proposed that the typologic study of zircon populations from granitic rocks can be used as a genetic classification, with three main divisions as (a) granitoids of crustal origin, (b) hybrid (crustal and mantle origin) granitoids, and (c) granitoids of mantle origin. On the typology diagram, granitoids of

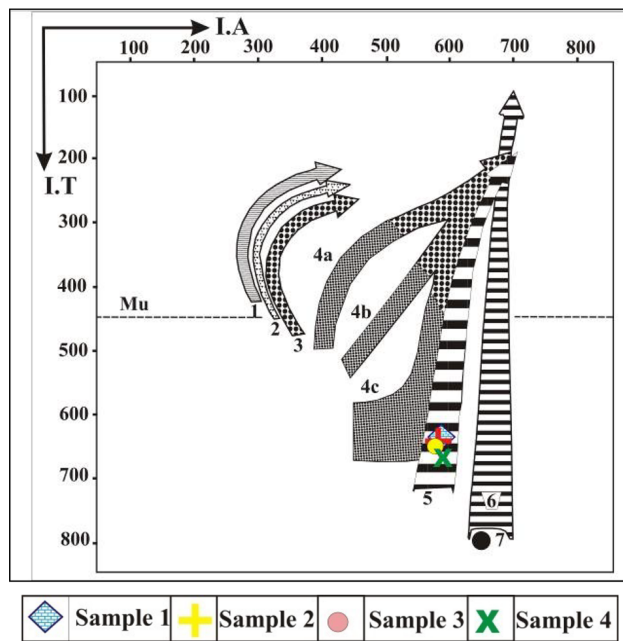


Fig. 12 Distribution of mean points and mean typological evolutionary trends of zircon populations (Pupin 1980) from: Aluminous anatetic granites 1 aluminous leucogranites; 2 (par) autochthonous monzogranites and granodiorites; 3 intrusive aluminous monzogranites and granodiorites. –Hybrid granites of crustal + mantle origin: (4a, b, c) calc-alkaline series granites (dark dotted area = granodiorites + monzogranites; clear dotted area = monzogranites + alkaline granites); 5 sub-alkaline series granites; 6 alkaline series granites; 7 tholeiitic series granites –Mu = limit of the muscovite granites (I.T. = 450)

different origin show different zircon populations and distinct T.E.T.'s (Pupin 1980).

The zircon typology method (Pupin 1980), based on the external morphology of zircon crystals was applied to some syenogranitic dykes in the study area. The analysis indicates that the major zircon types are S₂₀ and S₂₅, while the S₂₄ and S₁₅ types are less dominant. P₅, S₁₄, and S₁₉ types are present in minor amount in syenogranitic dykes

(Fig. 11). The typologic distribution has been determined and the coordinates in I.A. and I.T. (temperature index) space are computed (Pupin 1980), for the chosen four samples I.A. (1) = 588, I.A. (2) = 584, I.A. (3) = 585, I.A. (4) = 584 with average I.A. \approx 585 and I.T. (1) = 625, I.T. (2) = 632, I.T. (3) = 632, I.T. (4) = 662 with average I.T. \approx 637 (Fig. 11). The results of mean point of the investigated zircon grains of syenogranite dykes are plotted on the diagram (Fig. 12). Morphology of the studied zircon crystals suggests that, these zircon crystals were crystallized at mean temperature of \approx 637 °C and belong to sub-alkaline series granites.

4 Chemistry of zircon

The chemical compositions of the studied nine zircon samples are given in Table 1. Figure 13 shows the variation of oxides as well as HfO₂ to ZrO₂/HfO₂ in zircon separated from syenogranite dykes. Zircon crystals of the studied syenogranitic dykes show slightly differences in ZrO₂, SiO₂, HfO₂, UO₂, ThO₂ contents and similar contents of Al₂O₃, Fe₂O₃, CaO (Fig. 13d). Figure 13 e is showing a noticeable increasing of UO₂ contents comparing to ThO₂ contents which could be attributed to the hydrothermal processes and its accompanying uranium enrichment. Because the abundance of hafnium in the continental crust is low, about 3 ppm, (Taylor and McLennan 1985), no Hf mineral crystallizes during the solidification of magmatic rocks. Hf always occurs together with Zr due to their identical behavior and concentrated in zircon (Bau 1996). Hafnium tends to replace Zr, especially along crystal peripheries, during hydrothermal activity (Correia et al. 1974). On the diagram HfO₂-ZrO₂/HfO₂ (Fig. 13f), Hf content shows relative increasing consistent with the decreasing of Zr content, suggesting the replacement of Zr by Hf during hydrothermal activity.

Table 1 Chemical composition in percent of zircon separated from the studied syenogranite dykes

Sample no.	SiO ₂	ZrO ₂	HfO ₂	Al ₂ O ₃	Fe ₂ O ₃	CaO	UO ₂	ThO ₂	Total	ThO ₂ /UO ₂	HfO ₂ /ZrO ₂
1	33.26	64.42	0.37	0.11	0.17	0.51	0.37	0.18	99.39	0.49	0.006
2	34.21	63.36	0.39	0.18	0.16	0.42	0.51	0.23	99.46	0.45	0.006
3	33.21	64.82	0.47	0.12	0.16	0.41	0.54	0.22	99.95	0.41	0.007
4	33.24	64.41	0.38	0.12	0.18	0.53	0.39	0.19	99.44	0.49	0.006
5	33.68	63.14	1.47	0.14	0.15	0.51	0.48	0.26	99.83	0.54	0.02
6	33.11	64.45	0.36	0.11	0.16	0.43	0.58	0.26	99.46	0.49	0.006
7	33.45	63.46	1.41	0.12	0.18	0.46	0.52	0.24	99.84	0.46	0.02
8	33.24	63.52	0.92	0.13	0.44	0.47	0.88	0.28	99.88	0.39	0.01
9	34.11	63.14	1.22	0.11	0.15	0.43	0.57	0.24	99.97	0.42	0.02

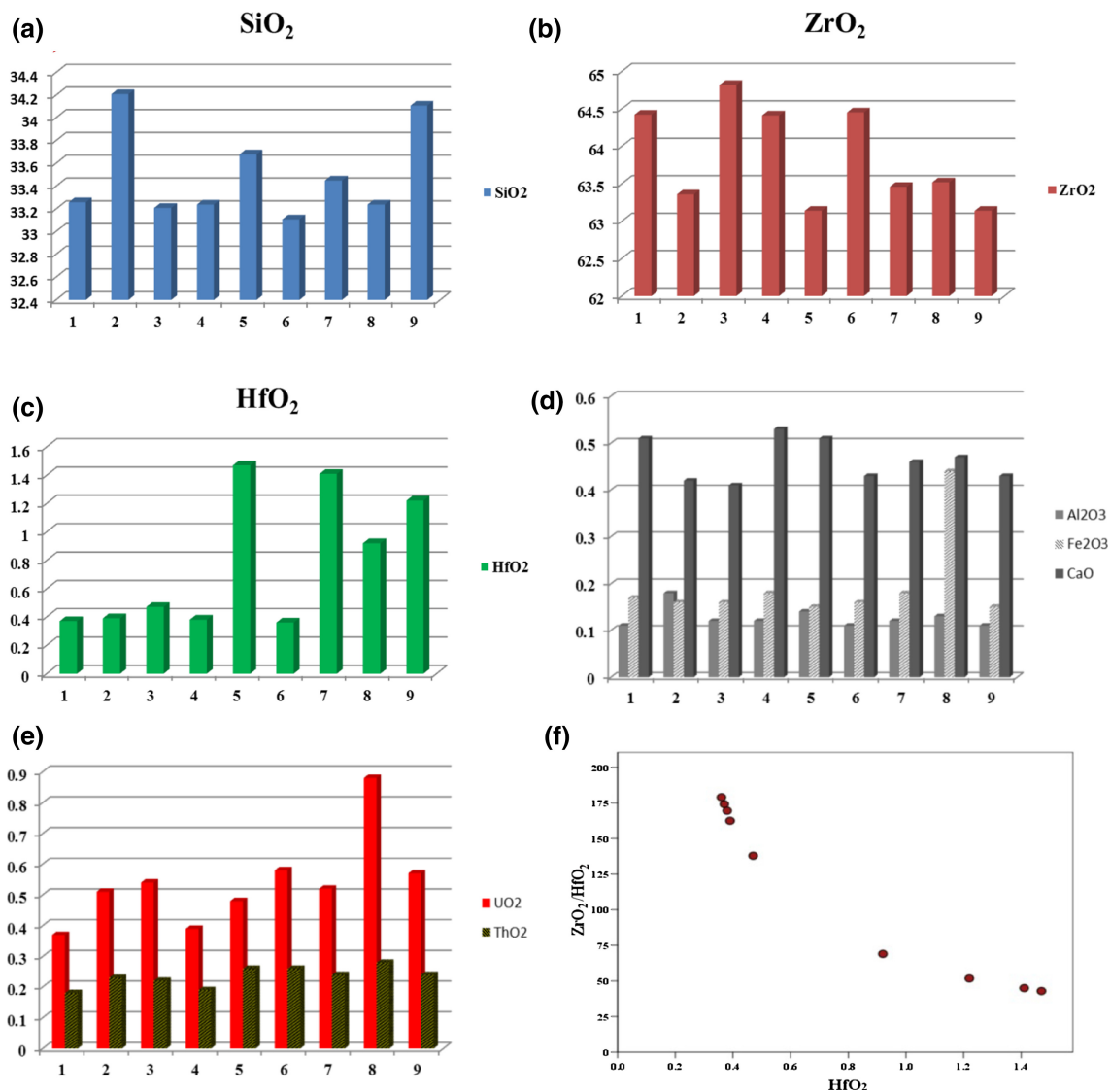


Fig. 13 Variation of oxides (wt.%) as well as $\text{HfO}_2\text{-ZrO}_2/\text{HfO}_2$ ratios, (from Wang et al. 1992), of zircon crystals separated from syenogarnite dykes

5 Radioactive mineralization

Th/U ratios for granitic rocks are thought to be normal if they are within the range of 3 to 5. Possible economic significance was proposed for granites with Th/U ratios either below or above this range (Nash 1979; Stuckless 1979). Post-magmatic hydrothermal processes reflected by their alteration imprints in the source rocks constitute the critical prerequisite for mobilization and redistribution of the primary magmatic uranium. Friedrich et al. (1987) discussed the various modes of hydrothermal source rock alteration in the light of its efficiency in mobilization of uranium. Solution which controlled uranium liberation takes place essentially along zones of fracturing and cataclasis that provide the

transmissivity needed as pathways for the fluids. The nature of the fluids may vary between hypogene hydrothermal and supergene meteoric. Favorable sites of adequate permeability are restricted to brittle structures, transcurrent ductile mylonite zones, and marginal segments of granitic dykes (Lespinasse and Pecher 1986).

Through ground gamma ray spectrometric study, it has been observed that the late-stage syenogranitic dykes have the highest potential equivalent uranium and thorium exists comparing to the other exposed rock types in the study area.

The syenogranitic dykes show average equivalent uranium (eU) content 53.2 ppm, while the equivalent thorium (eTh) content is 228 ppm. The maximum contents of eU

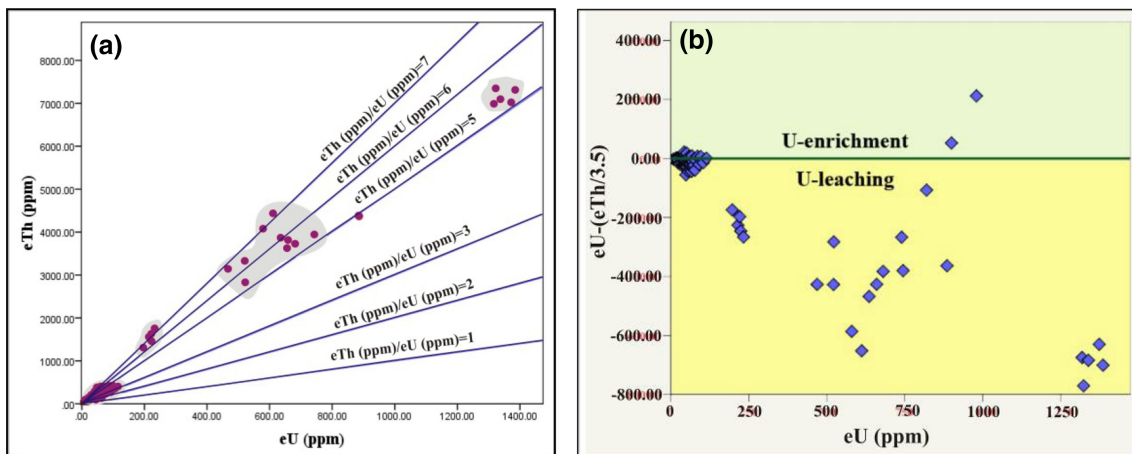
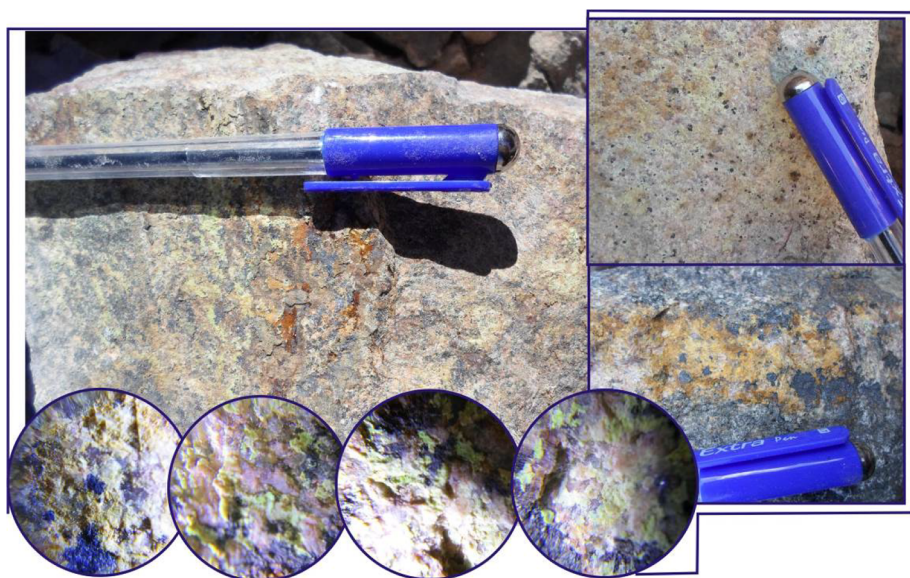


Fig. 14 **a** $e\text{U}$ (ppm) versus $e\text{Th}$ (ppm) plot diagram of the studied syenogranitic dykes. **b** Uranium mobilization in the studied dykes. The equation $e\text{U} - (e\text{Th}/3.5)$ reflects the uranium mobilization. If the result of this equation equals zero, it indicates absence or at least very restricted uranium mobilization. When it is greater than zero it means that uranium was enriched (added to rock). The *negative values* mean uranium leaching out

Fig. 15 Close up views showing visible uranophane and autunite



and $e\text{Th}$ are 114.3 ppm and 413 ppm, respectively. Generally, syenogranite dykes showing contents of uranium and thorium are higher than the normal granites contents. This could be attributed to the high magma content of these elements (magmatic origin).

The mineralized syenogranitic dykes are characterized by high uranium and thorium contents. They show thorium anomalies rather than the uranium where the $e\text{U}$ average is 707.2 ppm while that of $e\text{Th}$ is 4044 ppm. The maximum $e\text{Th}$ content exceeds to 7331 ppm while that of $e\text{U}$ reaches up to 1386 ppm. The mineralized zones occur as highly ferruginated, highly fractured and highly altered irregular bodies or patches confined to shear and fault planes at the

contact area and also clearly observed as fracture filling on the walls of dykes. The noticeable increasing of $e\text{Th}$ content comparing to $e\text{U}$ in mineralized zones (Fig. 14a, b), probably represent mobilization and redeposition of uranium by supergene processes, (including the predominance of meteoric water circulation), and accumulated near to the contacts of impermeable parts. The presence of the iron oxy-hydroxides alteration, which is the main alteration process, couldn't be ignored. This may be due to the high ability of iron oxides to adsorb uranium from its bearing solutions and/or the prevalence of oxidation conditions and complexing ions that cause precipitation of uranium as complex uranyl ions (Hussein et al. 1965). Visible

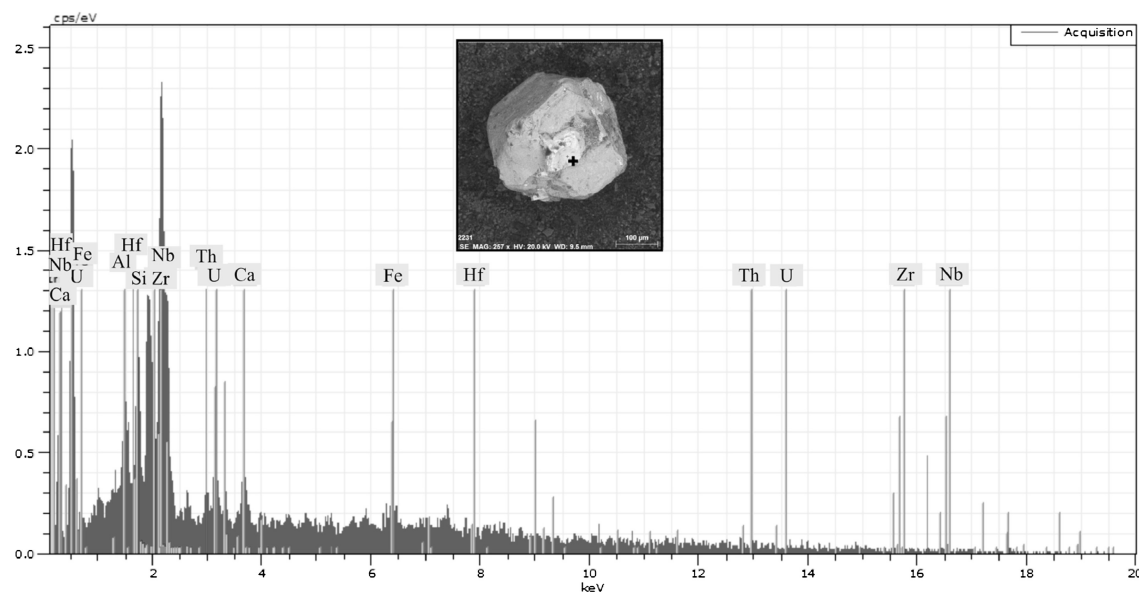
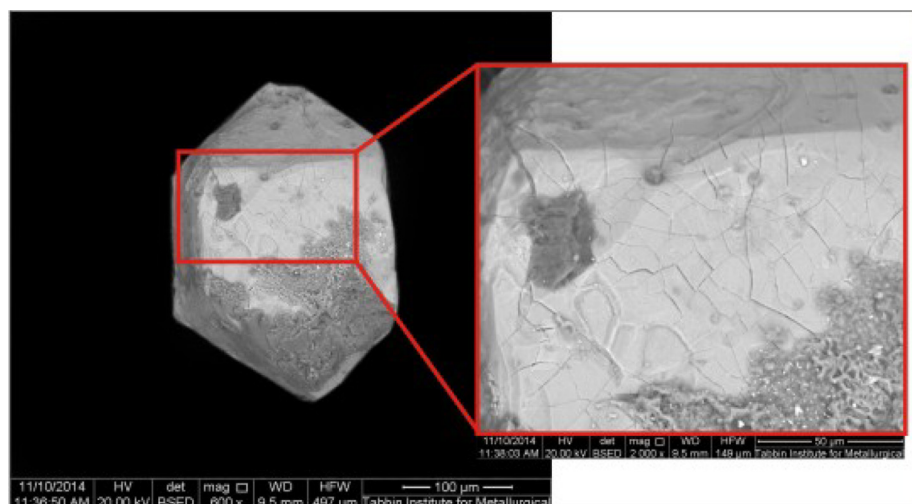


Fig. 16 EDX and BSE images of thorite, uranothorite, uranophane and columbite as inclusions in zircon

Fig. 17 SEM photomicrograph shows the volume expansion of the U-rich metamict domain



mineralization is present and recognized by the presence of uranophane and autunite as well as thorium minerals and thorium bearing minerals such as thorite, uranothorite and columbite (Figs. 15 and 16).

Metamictization is the process of lattice destruction by radiation damage (Williams 1992), and it occurs at temperature conditions at which annealing of the lattice is slower than the damage accumulates, and therefore more severe in zircon with high U and Th concentrations bond angles in zircon, which tends to be amorphous at full metamictization (Nasdala et al. 2001). Some of zircon crystals that we studied have significant metamictization as results of uranium and thorium atoms substituting for zirconium in the crystal structure (Fig. 17).

6 Discussion and conclusions

Ra's Abdah area is located approximately 20 km to the southwest Safaga City on the Red Sea, north Eastern Desert of Egypt, and is limited by latitudes $26^{\circ}42'50''$ and $26^{\circ}44'28''N$ and longitudes $33^{\circ}44'51''$ and $33^{\circ}47'59''E$. It is occupied by older granitoids, younger gabbro, younger granites and dyke phases. Syenogranitic dykes outcrop dimensions range from few meters to hundred meters in length and from less than a meter up to tens of meters in width. The separated zircon grains from syenogranitic dykes have no wide range of colour which are ranging from pale yellow, bright yellow, honey and brown with some crystals showing significant overgrowth.

Despite of the widely accepted (Pupin 1980) classification of zircon typology; however we find that zircon from a single rock population can have widely varying morphologies. According to the proposed petrogenetic classification of Pupin (1980), the investigated zircons of syenogranite dykes belong to Sub-alkaline series granites and crystallized at mean temperature of about 637 °C. In this study, we recognize different distinct zircon types on the basis of host rock and texture: (1) magmatic zircons, hosted by intrusive igneous rocks; (2) hydrothermal (or late-magmatic) overgrowths of zircon, associated with magmatic type. All the types have been observed in samples from syenogranitic dykes. Syenogranite dykes which have been emplaced at the late-magmatic phase are rich in radioactive mineralization reflecting the high background measurements. These dykes have been subjected to hydrothermal solutions rich in uranium and thorium elements evidenced by zircon overgrowth.

Zircon chemistry revealed a relative increasing of Hf contents consistent with the decreasing of Zr contents suggesting replacement of Zr by Hf during hydrothermal activity. Some of zircon crystals have significant metamictization as results of uranium and thorium atoms substituting for zirconium in the crystal structure. The studied zircon crystals are characterized by the presence of high inclusions of thorite, uranophane and columbite minerals.

At some mineralized parts the maximum eTh content exceeds 7331 ppm while that of eU reaches up to 1386 ppm. Visible uranium mineralization is present and recognized by the presence of uranophane and autunite.

References

- Bau M (1996) Controls on the fractionation of isovalent trace elements in magmatic and aqueous systems; evidence from Y/Ho, Zr/Hf, and lanthanide tetrad effect. *Contrib Mineral Petrol* 123:323–333
- Bineli Betsi T, Lentz DR (2010) The nature of “quartz eyes” hosted by dykes associated with Au-Bi-As-Cu, Mo-Cu, and base-metal-Au-Ag mineral occurrences in the Mountain Freegold region (Dawson Range), Yukon, Canada. *J Geosci* 55:347–368
- Breiter K (2002) From explosive breccia to unidirectional solidification textures: magmatic evolution of a phosphorus- and fluorine-rich granite system (Podlesí, Krusné hory Mts., Czech Republic). *Bull Czech Geol Surv* 77:67–92
- Cemal Köksal S, Göncuoglu M, Toksoy-Köksal F, Möller A, Kemnitz H (2008) Zircon typologies and internal structures as petrogenetic indicators in contrasting granitoid types from central Anatolia, Turkey. *Mineral Petrol* 93:185–211
- Corfu F, Hanchar JM, Hoskin PWO, Kinny P (2003) Atlas of zircon textures. In: Hanchar JM, Hoskin PWO (eds) *Zircon. Reviews in mineralogy and geochemistry*. Mineralogical Society of America, Chantilly
- Correia NJM, Lopes NJE, Sahama ThG (1974) High hafnium member of zircon-hafnon series from the granite pegmatites of Zambezia, Mozambique. *Contr Min Petr* 48:73–80
- Dardier AM (1999) Morphology and geochemistry of zircon associated with uranium mineralization in Gattar granitic pluton, north Eastern Desert, Egypt. *J Mineral Soc Egypt* 11:91–104
- Derre C, Lecolle M, Roger G, de Freitas Tavares, Carvalho J (1986) Tectonics, magmatism, hydrothermalism and sets of flat joints locally filled by Sn-W aplite-pegmatite and quartz veins; southeastern border of the Serra de Estrela granitic massif (Beira Baixa, Portugal). *Ore Geol Rev* 1:43–56
- El-Mansi MM, Dardier AM, Abdel Ghani IM (2004) Crystal habit and chemistry of zircon as a guide for uranium redistribution in Gabal Ria El-Garrah area, Eastern Desert, Egypt. *Delta J Sci* 28:19–30
- Friedrich M, Cuney M, Pory B (1987) Friedrich M, Cuney M, Pory B (1987) Uranium geochemistry in peraluminous leucogranites, in: concentration mechanisms of uranium in geological environments: a conference report. *Uranium* 3:353–358
- Gastil RG, DeLisle M, Morgan J (1967) Some effects of progressive metamorphism on zircons. *Geol Soc Am Bull* 78(7):879–906
- Hussein HA, Faris MI, Makram W (1965) Radioactivity of some accessory minerals especially zircon in some Egyptian granites and pegmatites. *J Geol UAR* 9(2):13–16
- Kroner A, Eyal M, Eyal Y (1990) Early Pan-African evolution of the basement around Elat, Israel, and the Sinai Peninsula revealed by single-zircon evaporation dating, and implications for crustal accretion rates. *Geology* 18:545–548
- Lentz DR (2005) Examination of dikes in ore-forming systems: analysis of geological, petrochemical, and geotectonic constraints. *Actas Del XVI Congr Geol Argent*, LaPlata, pp 403–411
- Lespinasse M, Pecher A (1986) Microfissuration and regional stress field: a study of the preferred orientation of fluid inclusion planes in a granite from the Massif Central, France. *J Struct Geol* 8:169–180
- Moore JM (1975) A mechanical interpretation of the vein and dyke systems of the S.W. England Ore field. *Mineral Deposita* 10:374–388
- Nasdala L, Beran A, Libowitzky E, Wolf D (2001) The incorporation of hydroxyl groups and molecular water in natural zircon ($ZrSiO_4$). *Am J Sci* 301:831–857
- Nash JT (1979) Uranium and thorium in granitic rocks of northeastern Washington and northern Idaho, with comments on uranium resource potential: U.S. Geological Survey Open-File Rept. 79–233, p 39
- Omran AA (2005) Geological, petrochemical studies and potentiality of uranium-thorium occurrences in Gabal Um Taghir El-Tahtani area with emphasis on the granitic rocks, Central Eastern Desert, Egypt. Ph.D. thesis, Ain Shams University Cairo p 189
- Omran AA (2015) Geology, mineralogy and radioelements potentiality of microgranite dikes to the south of wadi abu hadieda area, northern eastern desert. *In press*
- Pupin JP (1980) Zircon and granite petrology. *Contrib Mineral Petr* 73:207–220
- Pupin JP, Bunin B, Tessier M, Turco G (1978) Role de l'eau sur les caractères morphologiques, et la cristallisation du zircon dans les granites. *Bull Soc Geol Fr* 20:721–725
- Rubin JN, Henri CD, Price JG (1989) Hydrothermal zircons and zircon overgrowths, Sierra Blanca Peaks, Texas. *Am Mineral* 74:865–869
- Stein M, Goldstein SL (1996) From plume head to continental lithosphere in the Arabian-Nubian shield. *Nature* 383:773–778
- Štemprok M, Seifert T, Holub FV, Chlupáčová M, Dolejš D, Novák JK, Pivec E, Lang M (2008) Petrology and geochemistry of Variscan dykes from the Jáchymov (Joachimsthal) ore district, Czech Republic. *J Geosci* 53:65–104
- Stern RJ, Hedge CE (1985) Geochronologic and isotopic constraints on late Precambrian crustal evolution in the Eastern desert of Egypt. *American Journal Science* 285:97–127

- Stern RJ, Gottfried DG, Hedge CE (1984) Late Precambrian rifting and crustal evolution in the North Eastern Desert of Egypt. *Geology* 12:168–172
- Stuckless JS (1979) Uranium and thorium concentrations in Precambrian granites as indicators of a uranium province in central Wyoming. *Contrib Geol* 17(2):173–178
- Taylor SR, McLennan SM (1985) The continental crust: its composition and evolution. Blackwell Scientific Publication, Carlton n, p 312
- Vallance J, Cathelineau M, Boiron MC, Fourcade S, Shepherd TJ, Naden J (2003) Fluid-rock interactions and the role of late Hercynian aplite intrusion in the genesis of the Castromil gold deposit, northern Portugal. *Chem Geol* 194:201–224
- Wang RC, Fontan F, Monchoux P (1992) Minéraux disséminés comme indicateurs du caractère pegmatitique du granite de Beauvoir, massif d'Échassières, Allier, France. *Can Mineral* 30:763–770
- Williams IS (1992) Some observations on the use of zircon U-Pb geochemistry in the study of granitic rocks. *Trans R Soc Edinb* 83:447–458